PBVHx-based microspheres for controlled BMP2 release and enhanced bone regeneration in a disuse osteoporosis mouse model

Kewen Zhang[1,2#], Yanwen Zhou[3#], Daixu Wei[3*], Airong Qian[4*], and Xiao Lin[1,4*]

ABSTRACT

Addressing bone defects caused by degenerative diseases, trauma, and cancer through bone tissue engineering remains a significant global health challenge. The osteoinductive properties of bone morphogenetic protein-2 (BMP2) have become a key therapeutic strategy in bone regeneration. However, the development of biodegradable composites that ensure biocompatibility, stability, efficient BMP2 loading, and controlled release remains unresolved. In this study, we designed PBVHx/soy lecithin (SL)/BMP2 controlled-release microspheres (sB2PM) based on the biodegradable material poly(3-hydroxybutyrate-co-3-hydroxyvalerate-co-3-hydroxyhexanoate) (PBVHx), incorporating SL to enable sustained BMP2 delivery and enhance capture. sB2PM microspheres exhibited uniform size (approximately 5 μm) and high BMP2 encapsulation efficiency (80.29%) compared to pure PBVHx-based microspheres (pPM). Due to PBVHx's biodegradability, BMP2 release was primarily degradation-driven, resulting in a controlled biphasic release profile. sB2PM achieved 62.79% cumulative BMP2 release over four weeks and continued to release BMP2 sustainably thereafter. Co-culturing sB2PM microspheres with human bone marrow-derived mesenchymal stem cells (hBMSCs) in a Transwell system showed enhanced cell proliferation, biocompatibility, and collagen secretion. Compared with pPM and B2PM, sB2PM significantly promoted osteogenic differentiation, increased alkaline phosphatase (ALP) activity, and upregulated osteogenic gene expression in hBMSCs, outperforming commercial hydroxyapatite microspheres. In a mouse hindlimb unloading osteoporosis model, micro computed tomography and histological evaluations confirmed that injectable sB2PM microspheres significantly enhanced bone regeneration, collagen secretion, and ALP and runt-related transcription factor 2 protein expression. This study highlights the potential of sB2PM microspheres with controlled BMP2 release for future bone regeneration therapies.

Keywords:
Polyhydroxyalkanoates; Osteoporosis; Controlled release microspheres; Bone morphogenetic protein-2; Mesenchymal stem cells

#Authors contributed equally.

*Corresponding authors:
Xiao Lin,
linxiao@nwpu.edu.cn;
Airong Qian,
qianair@nwpu.edu.cn;
Daixu Wei,
weidaixu@cdu.edu.cn

1. Introduction

Osteoporosis is a metabolic bone disease caused by an imbalance between bone formation and bone resorption. It is characterized by the deterioration of bone microstructure, decreased bone mass, and poor bone regeneration ability, which collectively increase the risk of fractures.[1-5] The disease commonly affects astronauts returning from space missions, the elderly, and postmenopausal women. At present, over one billion people worldwide are affected by osteoporosis.[6,7] With the aging global population, the number of patients is expected to increase, placing a significant burden on society.[8-11] In clinical treatment, nearly half of osteoporosis patients discontinue treatment due to poor adherence. The main contributing factors include inconvenient drug administration, side effects, and a lack of motivation to continue therapy.[12-14] To address the challenge of long-term and frequent drug administration, long-acting

sustained-release drug delivery systems offer an effective method.[15,16]

Bone morphogenetic proteins (BMPs) play key roles in cartilage and bone development, as well as bone regeneration.[17] Among them, BMP2 promotes osteogenic differentiation by inducing progenitor cells to mature into osteoblasts and by enhancing the production and mineralization of extracellular matrix (ECM), which forms the structural framework of bone tissue.[8,18,19] Studies on BMP2-deficient mice have revealed severe impairments in osteoblast proliferation, differentiation, and bone repair, highlighting the essential role of BMP2 in osteogenesis.[20] During bone development, BMP2 and Wnt signaling pathways jointly regulate runt-related transcription factor 2 (RUNX2) and osterix 1 in bone/cartilage progenitor cells and are involved in every stage of endochondral osteogenesis. BMP2 also regulates several osteogenesis-related genes, including *Osx*, *Wnt1*, *Lrp5*, and *Axin2* via the Wnt signaling pathway.[21] Due to its strong ability to promote bone repair, especially in critical-sized defects, the United States Food and Drug Administration approved recombinant human BMP2 for clinical use in spinal fusion and tibial axis repair in 2002.[22] However, as a growth factor, BMP2 requires protection to maintain its biological activity. In clinical applications, its short half-life and rapid degradation significantly limit its therapeutic efficacy in promoting bone regeneration.[23] Therefore, the development of a long-acting, bioactive BMP2 delivery system based on sustained-release biomaterials is of great importance.

Polyhydroxyalkanoates (PHAs) are a class of polymers synthesized by microbial fermentation that can be processed into various composite material forms and exhibit excellent processing properties. Due to their favorable biocompatibility and biodegradability, PHAs are widely used in the field of tissue engineering.[24-27] Different monomers allow PHAs to form a variety of complex structures, such as polyhydroxybutyrate (PHB), polyhydroxyvalerate, poly(3-hydroxybutyrate-co-3-hydroxyvalerate-co-3-hydroxyhexanoate) (PBVHx), poly(3-hydroxybutyrate-co-3-hydroxyhexanoate) (PHBHHx).[28] In bone tissue engineering, PHAs have shown the ability to promote osteogenic differentiation and bone regeneration. 3-hydroxybutyric acid (3HB), a degradation product of PHA, can enhance osteogenic differentiation, inhibit bone resorption, and restore bone microstructure and mechanical properties in ovariectomized and simulated microgravity-induced osteoporosis models.[29-31] Nanocomposite scaffolds composed of PHB, zein, and multiwalled carbon nanotubes, fabricated via electrospinning, have been shown to promote MG-63 cell proliferation, osteogenic gene expression, and alkaline phosphatase (ALP) secretion.[32] PHA porous microspheres also support human bone marrow-derived mesenchymal stem cells (hBMSC) adhesion, osteogenic differentiation, and *in vitro* bone tissue regeneration.[33]

P(3HB-co-4HB) has demonstrated the ability to promote osteogenic differentiation of hBMSCs and vascularized bone regeneration in rat skull defect models.[34] PBVHx, the newest PHA trimer, is composed of 3-hydroxybutyrate (HB), 3-hydroxyvalerate (HV), and 3-hydroxycaproate (HHx). It exhibits excellent biocompatibility and has shown promise in cartilage repair and liver regeneration applications.[35,36] Compared with other PHA materials, such as PHB, PHBV, and PHBHHx, PBVHx offers distinct advantages in flexibility, degradability, and biocompatibility.[37] Recently, PBVHx has been used for the long-term delivery of Huperzine A in Alzheimer's disease[38] and for the sustained release of BMP4 and BMP6 to promote osteogenic differentiation of hBMSCs.[39,40] Its controlled degradation properties make PBVHx particularly suitable for bone tissue engineering applications,[41] enhancing its potential as a long-acting delivery system for bioactive BMP2. However, the biological effects of PBVHx loaded with BMP2 on osteogenic differentiation and bone defect repair remain unclear.

Here, we designed and synthesized a biocompatible and bioresorbable PBVHx/soy lecithin (SL)/BMP2 controlled-release platform (sB2PM) with enhanced BMP2 loading capacity, sustained release behavior, good biocompatibility, and effective bone regeneration potential in a hindlimb unloading (HLU)-induced osteoporotic mice (**Figure 1**). PBVHx-based microspheres, including pure PBVHx-based microspheres (pPM), B2PM, and sB2PM, were prepared using a microfluidic platform. These microspheres enable precise and continuous release of active BMP2, specifically designed to promote directed osteogenic differentiation of stem cells and new bone formation. The biocompatibility of sB2PM in hBMSCs, along with its effects on ECM secretion, ALP activity, and osteoinductive properties, was investigated *in vitro*. *In vivo*, the effects of sB2PM on bone regeneration and osteogenic protein expression were evaluated in a disuse osteoporosis mouse model. The design and development of this multifunctional PBVHx-based biodegradable platform, capable of controlled BMP2 release, may provide an effective strategy for the targeted treatment of osteoporotic bone defects.

2. Materials and methods

2.1. Materials

Poly(3-hydroxybutyrate-co-3-hydroxyvalerate-co-3-hydroxyhexanoate) (molecular weight 25,000 Da; composition: 85 mol% 3HB, 2 mol% 3HV, and 12 mol% 3HHx) was acquired from Bluepha Co., Ltd. (China). Commercial hydroxyapatite microspheres (HApM) were purchased from LEANTON Co., Ltd. (China). Recombinant human BMP 2 was sourced from R&D Systems (United States of America [USA]). SL containing 70–97% phosphatidylcholine was purchased from Shanghai Tai-wei Pharmaceutical Co., Ltd. (China). Poly(vinyl alcohol)

[1]Shenzhen Research Institute of Northwestern Polytechnical University, Shenzhen, Guangdong, China; [2]The Second Affiliated Hospital, School of Medicine, The Chinese University of Hong Kong, Shenzhen and Longgang District People's Hospital of Shenzhen, Shenzhen, Guangdong, China; [3]Clinical Medical College and Affiliated Hospital of Chengdu University, Chengdu University, Chengdu, Sichuan, China; [4]Key Lab for Space Biosciences and Biotechnology, School of Life Sciences, Northwestern Polytechnical University, Xi'an, Shaanxi, China
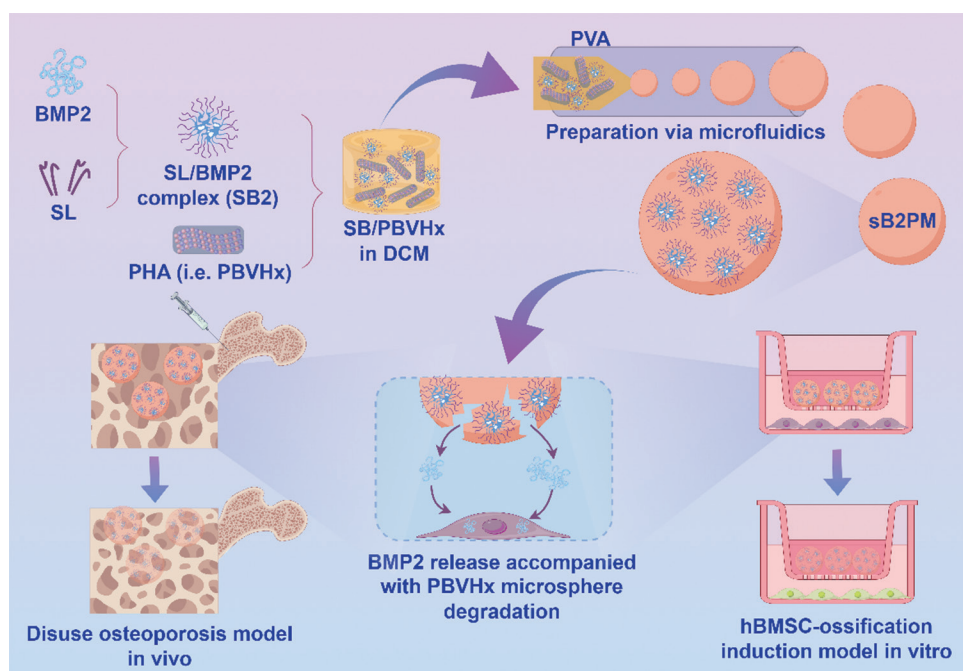
Figure 1. Schematic illustration of the preparation of the PBVHx platform and its effects on hBMSC proliferation, ECM secretion, and osteogenic differentiation *in vitro*, as well as its therapeutic role in bone regeneration in a hindlimb unloading-induced osteoporosis mouse model *in vivo*. The illustration was created using Figdraw.

Abbreviations: BMP2: Bone morphogenetic protein-2; DCM: Dichloromethane; ECM: Extracellular matrix; hBMSC: Human bone marrow-derived mesenchymal stem cells; PHA: Polyhydroxyalkanoate; PVA: Poly(vinyl alcohol); PBVHx: Poly(3-hydroxybutyrate-co-3-hydroxyvalerate-co-3-hydroxyhexanoate); sB2PM: PBVHx/soy lecithin (SL)/BMP2 controlled-release microspheres; SL: Soy lecithin.

(PVA; 87–89% hydrolyzed, with an average molecular weight of 13,000–23,000 Da) was obtained from Sigma-Aldrich (USA). All other chemicals used were of analytical grade and were procured from Sinopharm Chemical Reagent Co., Ltd. (China).

2.2. Preparation of SL–BMP 2 complex

The SL-BMP2 complex (sB2) was prepared using a physical blending approach. Specifically, SL and BMP2, in a weight ratio of 5:1, were dissolved in dimethyl sulfoxide containing 5% (v/v) acetic acid and stirred magnetically at 30°C for 24 h. The resulting mixture was subsequently lyophilized for 12 h to remove the solvent. The obtained sB2 was hermetically sealed and stored at 4°C for subsequent use.

2.3. Fabrication of SL–BMP 2 complex-loaded PBVHx-based microspheres

SL-BMP2-loaded PBVHx-based microspheres were fabricated using a microfluidic platform. A solution containing 0.01 g BMP2 (in the form of sB2) and 0.25 g PBVHx was prepared in 5 mL of dichloromethane (DCM). An aqueous PVA solution (0.1% w/v) was prepared by dissolving 0.1 g PVA in 100 mL ultrapure water at 80°C for 2 h. During fabrication, the internal phase, consisting of PBVHx/DCM, was conveyed through the injection capillary, while the external phase (PVA) was guided through the channel of the square capillary channel, resulting in the formation of a single oil-in-water emulsion droplet within the collection capillary. The flow rates of the internal phase (400 mL/h) and the external phase (2,000 mL/h) were precisely controlled using two distinct syringe pumps (LSP01-2A; Longer Pump Inc., China). Subsequently, the

collected droplets were transferred into a petri dish containing a 0.1% (w/v) PVA aqueous solution. After evaporation of the DCM at ambient temperature overnight, the PBVHx microspheres were thoroughly rinsed with deionized water to remove any residual PVA. The sB2PMs were collected through centrifugation at 800 rpm for 5 min, washed three times with ultrapure water, and stored at 4°C. Control microspheres were prepared using the same method, but either with untreated BMP2 (pB2) or without BMP2 (pPM).

2.4. Morphology and size measurements of PBVHx-based microspheres

The morphology of PBVHx-based microspheres was examined using scanning electron microscopy (SEM; Hitachi S-4800, Japan) at an accelerating voltage of 5 kV. The mean microsphere size and distribution were determined using a Mastersizer 2000 (Malvern, United Kingdom [UK]) at room temperature.

2.5. Entrapment efficiency measurements of PBVHx-based microspheres

The entrapment efficiency of BMP2 was assessed using a modified centrifugation method.[42] The supernatant obtained after centrifugation was analyzed for free BMP2 using enzyme-linked immunosorbent assay (ELISA) and phospholipid assay kits. Entrapment efficiency was calculated using Equation I:

Entrapment efficiency (%) =(Wt − Wf)/Wt × 100%   (I)

where Wf and Wt represent the content of collected free BMP2 and the total amount of BMP2 used during preparation, respectively.

2.6. Water uptake rate and porosity measurements of PBVHx-based microspheres

The hydrophilicity of PBVHx-based microspheres was assessed by measuring the water uptake rate. Dried microspheres were immersed in ultrapure water at room temperature for 72 h. The water uptake rate was calculated using Equation II:

$$WUR\ (\%) = (Ww - Wd)/Wd \times 100\% \qquad (II)$$

where Ww and Wd are the wet weight and dry weight of the scaffolds, respectively, and (Ww – Wd) represents the amount of water absorbed by the scaffolds. Each measurement was performed in quadruplicate ($n = 4$).

To evaluate the internal space within various scaffolds, porosity was measured as described in previous studies. After lyophilization for 12 h, the dried scaffolds were immersed in absolute ethanol at room temperature for 10 min. Porosity was calculated using Equation III:

$$Porosity\ (\%) = (V0 - V1)/(Vt - V1) \times 100\% \qquad (III)$$

where V0 is the initial volume of absolute ethanol added to the dried scaffolds, Vt is the total volume of the system after immersion, and V1 is the volume of the residual ethanol after removing the liquid-impregnated scaffolds. Each measurement was performed in quadruplicate ($n = 4$).

2.7. Distribution of BMP 2 in PBVHx-based microspheres

Microsphere samples were fixed, permeabilized, and blocked before incubation with primary and secondary antibodies specific to BMP2. Images showing the distribution of BMP2 were obtained using confocal laser scanning microscopy (CLSM; Nikon, Japan).

2.8. *In vitro* degradation and BMP 2 release studies of PBVHx-based microspheres

To evaluate degradation behavior, 10 mg of PBVHx-based microspheres were immersed in 10 mL of degradation medium at 37C° for 32 days. The degradation medium consisted of phosphate-buffered saline (PBS; pH 7.4) supplemented with 1 mg/mL lipase. The medium was refreshed every four days to maintain lipase activity. At the designated time points, the residual PBVHx-based microspheres were air-dried at 25°C for 24 h and weighed. The degradation medium was also collected. The weight residual ratio of all dried microspheres was calculated using Equation IV:

$$Weight\ residual\ ratio\ (\%) = (Wres/Wtot) \times 100\% \qquad (IV)$$

where Wres and Wtot represent the weight of the residual and total PBVHx-based microspheres, respectively. Each measurement was performed in triplicate ($n = 3$).

Similarly, 100 mg of PBVHx-based microspheres were immersed in 50 mL of degradation medium at 37°C for 32 days to assess BMP2released. The release medium was periodically replaced, and the amount of released BMP2 was quantified using ELISA and phospholipid assay kits.

2.9. Cell culture on PBVHx-based microspheres

hBMSCs were obtained from Cyagen (China). The cells were cultured in Dulbecco's Modified Eagle's Medium supplemented with 10% fetal bovine serum (HyClone, USA), 100 U/mL penicillin, and 100 µg/mL streptomycin. The culture was maintained at 37°C in a humidified atmosphere containing 5% carbon dioxide (CO_2).

A total of 2×10^6 hBMSCs were suspended in 0.8 mL of basal medium (BM, devoid of any osteogenic factors) and seeded onto tissue culture plates (TCPs) containing PBVHx-based microspheres or a similar amount of HApM on transwells. The cells were incubated for 24 h at 37°C under 5% CO_2. Cell viability was evaluated using a Cell Counting Kit-8 (CCK-8) assay kit (Dojindo, Japan). At pre-determined time points, the culture medium was aspirated and replaced with 1 mL of fresh BM containing 0.1 mL of CCK-8 solution per sample. After further incubation, 200 µL of supernatant was collected from each sample and transferred to a 96-well plate. Absorbance was measured at 450 nm using a microplate reader (Multiskan MK3; Thermo Lab Systems, Finland). Each sample was assessed in six replicates ($n = 6$).

2.10. *In vitro* stem cell differentiation assay

The expression of collagen type I (COL-1) in cells was visualized using an immunohistochemical staining kit (Invitrogen, USA) and observed via CLSM. Specifically, cells on TCPs were initially fixed with 4% paraformaldehyde for 30 min. Permeabilization was then performed using 0.1% Triton X-100 for 15 min, followed by blocking with 3% bovine serum albumin (BSA; Sigma, USA) for 30 min. After blocking, hBMSCs were incubated with the primary antibody (Col1; catalog no.14695-1-AP; rabbit anti-human; Protentech, China) at 4°C overnight. This was followed by incubation with the secondary antibodies (Alexa488-conjugated donkey anti-rabbit; catalog no.A32790; Invitrogen, USA) for 1 h. The fluorescence intensity corresponding to Col1 was then analyzed.

To evaluate the osteogenic differentiation of hBMSCs, the expression of ALP was examined. After culturing the cells on scaffolds for 1, 7, and 14 days, the culture medium was removed. The scaffolds were washed three times with PBS to eliminate any residual medium. Then, 200 µL of 0.1% Triton X-100 was added and incubated for 10 min. The supernatants were subsequently collected to determine ALP activity and total protein content using an ALP activity kit (Shanghai Fusheng Biotechnology Development Co., Ltd., China) and a protein assay kit (Tiangen, China), respectively, according to the manufacturers' instructions. Each sample was measured in triplicate ($n = 3$).

To assess osteogenic differentiation and matrix mineralization in hBMSCs, the expression levels of osteogenic genes were analyzed 14 days post-seeding using quantitative real-time polymerase chain reaction (PCR) analysis, as previously reported. The QuantiTect SYBR Green PCR kit (Qiagen, Germany) was utilized to quantify the expression of four bone repair-related markers: *Runx2*, *Col1*, osteopontin (*Opn*), and osteocalcin (*Ocn*). Glyceraldehyde 3-phosphate dehydrogenase (*Gapdh*) was used as the internal reference gene. Primer sequences are presented in **Table 1**. Total RNA was extracted from the cells and used to synthesize complementary DNA, following the PCR kit instructions.

Table 1. Primer sequences used in quantitative real-time polymerase chain reaction

Gene	Forward (5'–3')	Reverse (5'–3')
Runx2	TTCTCCAACCCACGAATGCAC	CAGGTACGTGTGGTAGTGAGT
Col1	CCCAGAGTGGAACAGCGATT	ATGAGTTCTTCGCTGGGGTG
Opn	ACCAAAGTGAATGCCGAGAG	TCTGTGGTGAGGTTCGAGTG
Ocn	TCTGATGAGACCGTCACTGC	AGGTCCTCATCTGTGGCATC
Gapdh	GACTTCAACAGCAACTCCCAC	TCCACCACCCTGTTGCTGTA

2.11. Animal model

Eight-week-old male C57BL/6 mice (N = 30) were obtained from Charles River (China). For the HLU model, the mice were randomly divided into five groups (n = 6): ground control, HLU, HLU + pPM, HLU + sB2PM, and HLU + HApM. The ground control group was injected with PBS and allowed to move freely on the ground. In the HLU and HLU+sample groups, mice were injected with 200 μL of PBS or different samples into the bone marrow cavity of the mid-femur. The mice's tails were then suspended from the top of the cage, and each mouse was positioned with its head tilted downward at about 30°, allowing its forelimbs to move freely. After 4 weeks, femur samples were collected for further analysis. All animal experimental protocols were approved by the Medical and Laboratory Animal Ethics Committee of Northwestern Polytechnical University (China).

2.12. Micro-computed tomography analysis

The femurs were fixed in 4% paraformaldehyde, and the distal metaphyses were scanned using a Bruker SkyScan 1276 Micro-Computed Tomography (CT) system (USA). The scanning parameters were set as follows: Energy = 70 kV; current = 500 μA; angle increment = 0.2°; exposure time = 500 ms/step for 360 rotational steps; and resolution = 10 μm. A region of interest extending from the growth plate to 1.0 mm below the growth plate was selected for analysis using CTvox software (Blue Scientific, UK). Three-dimensional reconstruction was performed using NRecon Reconstruction software (Micro Photonics, USA). The following parameters were calculated: Bone mineral density (BMD; g/ccm), bone surface to tissue volume (BS/TV; 1/mm), bone surface area to bone volume ratio (BS/BV; 1/mm), bone volume to tissue volume ratio (BV/TV; %), trabecular number (Tb.N; 1/mm), trabecular pattern factor (Tb.Pf; 1/mm), and trabecular thickness (Tb.Th; mm).

2.13. Hematoxylin and eosin staining, Masson's trichrome staining, and immunohistochemical analysis

Femur tissues from the ground control, HLU, HLU + pPM, HLU + sB2PM, and HLU + HApM groups were decalcified in 10% ethylenediaminetetraacetic acid for four weeks. The tissues were then embedded in paraffin and sectioned into 4-μm-thick slices. Hematoxylin and eosin (H&E) staining was performed for histomorphological analysis, while Masson's trichrome (MT) staining was used to detect collagen distribution, as previously described.[43] For immunohistochemical analysis, the sections were subjected to antigen retrieval for 20 min and were blocked with 3% BSA for 30 min. The sections were then incubated with mouse primary antibodies against ALP (1:200) and RUNX2 (1:200) at 4°C overnight, followed by washing with PBS (2–3 times). Subsequently, sections were incubated with horseradish peroxidase-conjugated secondary immunoglobulin G (1:500) for 60 min. The DAB Horseradish Peroxidase Color Development Kit was used to visualize immunoreactivity. All images were captured using an Aperio AT2 Digital Whole Slide Scanner (Leica, Germany).

2.14. Statistical analysis

All data are presented as the mean ± standard deviation from parallel experiments. Statistical comparisons were conducted using Student's t-test or ANOVA. *$p < 0.05$ or **$p < 0.01$ was considered statistically significant. All statistical analyses were performed using GraphPad Prism 8 (GraphPad Software, USA).

3. Results

3.1. Characterization of various PBVHx-based microspheres

As shown in **Figure 1**, PBVHx-based microspheres were prepared using a microfluidic platform. The surface morphology of PBVHX-based microspheres was analyzed using SEM, and the results are shown in **Figure 2A**. The microspheres exhibited a relatively regular spherical shape. The surface of the pPM appeared slightly rough. After BMP2 loading, the surface of B2PM became smooth, while the surface of sB2PM displayed a distinct granular morphology, which may be attributed to the incorporation of SL and BMP2. The diameters of PBVHx-based microspheres were approximately uniform, mostly concentrated within the range of 4–9 μm (**Figure 2B**-**D**). The addition of BMP2 and SL did not significantly change the size of the microspheres.

As shown in **Figure 2E**, the entrapment efficiency of BMP2 in sB2PM (80.29%) was significantly higher than that observed in pPM (0%) or B2PM (16.08%), indicating that SL modification of BMP2 significantly enhances its entrapment efficiency with PBVHX-based microspheres compared to untreated BMP2. The hydrophilicity of PBVHX-based microspheres was evaluated by measuring their water absorption rate. A higher water absorption rate reflects greater hydrophilicity. The results showed the following order: sB2PM > B2PM > pPM (**Figure 2F**), indicating that the presence of SL or sB2 plays an important role in improving the hydrophilicity of PBVHX-based microspheres. In addition, the porosities of pPM, B2PM, and sB2PM were 11.98%, 14.35%, and 16.85%, respectively, with no significant differences observed among the groups (**Figure 2G**).
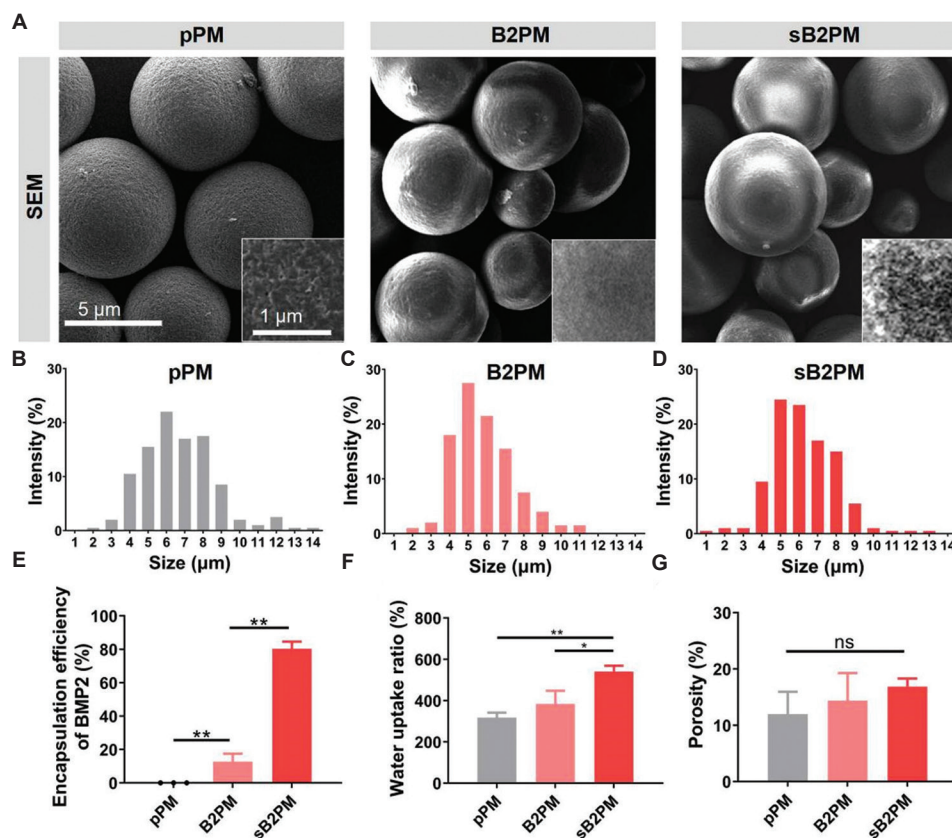
Figure 2. Characterization of various PBVHx microspheres. (A) Scanning electron microscopy images of pPM, B2PM, and sB2PM. Scale bars = 5 μm (large image) and 1 μm (insets). (B–D) Size and distribution analysis of the synthesized pPM, B2PM, and sB2PM. (E) Entrapment efficiency of BMP2 in pPM, B2PM, and sB2PM. (F) Water uptake ratios of pPM, B2PM, and sB2PM. (G) Porosity analysis of pPM, B2PM, and sB2PM. Data are presented as mean ± SD (n=3). *p<0.05, **p<0.01.
Abbreviations: BMP2: Bone morphogenetic protein-2; B2PM: PBVHx/BMP2 controlled-release microspheres; ns: Not significant; PBVHx: Poly(3-hydroxybutyrate-co-3-hydroxyvalerate-co-3-hydroxyhexanoate); pPM: Pure PBVHx-based microspheres; sB2PM: PBVHx/soy lecithin (SL)/BMP2 controlled-release microspheres.

3.2. Distribution and release of BMP 2 by sB2PM microspheres

BMP2 in PBVHx-based microspheres was visualized by immunofluorescent staining using antibodies against BMP2, and the microspheres were observed using CSLM, as shown in **Figure 3A**. The fluorescence intensity of the positive signal was quantified and compared (**Figure 3B**). Compared to B2PM, sB2 significantly increased the amount of BMP2 encapsulated on the surface of sB2PM microspheres by approximately 10.11-fold. Furthermore, the *in vitro* release of BMP2 was evaluated. During the 33-day degradation process, the three microspheres exhibited similar degradation behavior (**Figure 3C**). The BMP2 release profiles from pPM, B2PM, and sB2PM in PBS were assessed using dynamic dialysis technology (**Figure 3D**). B2PM demonstrated an initial burst release, with over 90% of the BMP2 released within the first 24 h. In contrast, sB2PM exhibited a unique biphasic release profile, with approximately 20% of BMP2 released within the first 24 h, followed by an extended and sustained release. Notably, about 40% of BMP2 remained in sB2PM even after 24 days. This biphasic release behavior is characterized by an initial burst attributed to the rapid elution of surface-associated sB2, followed by a sustained release phase driven by gradual microsphere degradation (**Figure 3E**).

3.3. *In vitro* cytotoxicity and biocompatibility of sB2PM microspheres

To assess the effects of sB2PM on the proliferative capacity of hBMSCs, pPM, B2PM, sB2PM, and commercial HApM were co-cultured with hBMSCs using a Transwell system (**Figure 4A**). The microspheres were placed in the upper chamber, while hBMSCs were seeded in the lower chamber to receive BMP2 released from the degrading microspheres. Cell viability was measured on days 1, 7, and 14 using the CCK-8 assay. As shown in **Figure 4B**, the proliferation capacity of hBMSCs co-cultured with sB2PM microspheres was significantly higher than that of cells co-cultured with pPM or B2PM microspheres at all-time points (days 1, 7, and 14), indicating that the controlled BMP2 release from sB2PM supports enhanced hBMSC proliferation. Notably, sB2PM exhibited the greatest proliferation-enhancing effect among all PBVHx-based microspheres. Although HApM significantly promoted cell proliferation at day 1, the effect of sB2PM became more pronounced on days 7 and 14 and surpassed that of HApM by day 14. Cell adhesion and growth were further evaluated by actin and immunofluorescence staining. Actin staining showed that hBMSCs treated with different microspheres exhibited good adhesion, with pseudopodia extended and displayed a long spindle-like shape (**Figure 4C**).
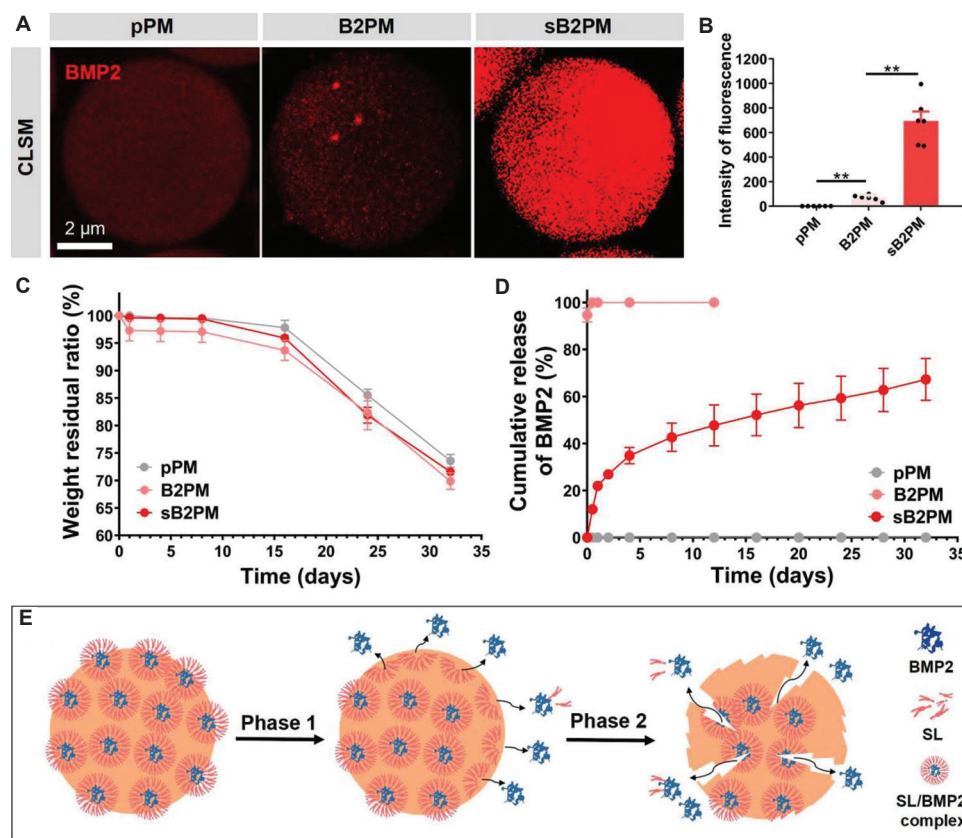
Figure 3. Distribution and release of BMP2 in PBVHx-based microspheres. (A) Confocal laser scanning microscopy images of BMP2 in pPM, B2PM, and sB2PM. Scale bar = 2 μm. (B) Quantification of BMP2 content based on red fluorescence intensity. (C) Weight residual ratios of pPM, B2PM, and sB2PM. (D) Cumulative release of BMP2 from pPM, B2PM, and sB2PM in PBS containing 1 mg/mL lipase. (E) Schematic illustration of the biphasic *in vitro* release behavior of BMP2 and SL from sB2PM. Data are presented as mean ± SD (n=3). *p<0.05, **p<0.01. Abbreviations: BMP2: Bone morphogenetic protein-2; B2PM: PBVHx/BMP2 controlled-release microspheres; PBVHx: Poly(3-hydroxybutyrate-co-3-hydroxyvalerate-co-3-hydroxyhexanoate); pPM: Pure PBVHx-based microspheres; sB2PM: PBVHx/soy lecithin (SL)/BMP2 controlled-release microspheres; SL: Soy lecithin.

In addition, the expression of the ECM component collagen, type I, alpha 1 (COL1A1) was highest in the sB2PM group compared to pPM, B2PM, and HApM (**Figure 4D**), confirming the excellent biocompatibility of sB2PM and their ability to promote ECM secretion.

3.4. Effect of sB2PM microspheres on osteogenic differentiation of hBMSCs *in vitro*

BMP2 is a critical inducer of bone development and repair.[17] Therefore, we further investigated the effect of sB2PM on the osteogenic differentiation of hBMSCs. hBMSCs were co-cultured with pPM, B2PM, sB2PM, and HApM for 1, 7, and 14 days, and osteogenic differentiation was evaluated by measuring ALP activity. Over time, pPM and B2PM showed no significant effect on ALP activity, whereas sB2PM and HApM significantly promoted ALP activity on days 7 and 14, with sB2PM demonstrating superior effects to HApM at day 14 (**Figure 5A**). In addition, the expression of osteogenic marker genes, including *Runx2*, Col1, Opn, and Ocn, was assessed by qPCR (**Figure 5B**-**E**). The results showed that sB2PM and HApM significantly upregulated the expression of these genes in hBMSCs after 7 and 14 days of co-culture, compared with pPM and B2PM. Notably, the effect of sB2PM was significantly greater than that of HApM, which can be attributed to the

continuous release of BMP2. These findings confirm that sB2PM exhibits strong osteoinductive effects *in vitro*.

3.5. Protective effects of sB2PM microspheres on bone loss in a disuse osteoporosis mouse model

To evaluate the therapeutic potential of sB2PM on bone loss *in vivo*, a disuse osteoporosis model was established in mice using HLU, with ground-fed mice serving as normal controls. PBS, pPM, sB2PM, and HApM were injected into the bone marrow cavity of the mid-femur in HLU mice to avoid damage to the cancellous bone structure below the growth plate. Treatment continued for four weeks. Ground control received PBS only (**Figure 6A**). Four weeks after HLU, femoral tissues were harvested for histological analyses, including micro-CT, H&E staining, MT staining, and immunohistochemistry. Micro-CT analysis showed that trabecular bone mass in the distal metaphyseal region of the femur was significantly reduced in HLU mice compared to the ground control group. However, sB2PM effectively mitigated bone loss and demonstrated superior efficacy compared to the other treatment groups (**Figure 6B**). Quantitative analyses of BMD, BS/TV, BS/BV, BV/TV, TB.N, TB.Pf, and Tb.Th further confirmed the superior therapeutic effects of sB2PM in alleviating disuse osteoporosis (**Figure 6C**-**I**). Cortical bone thickness, which
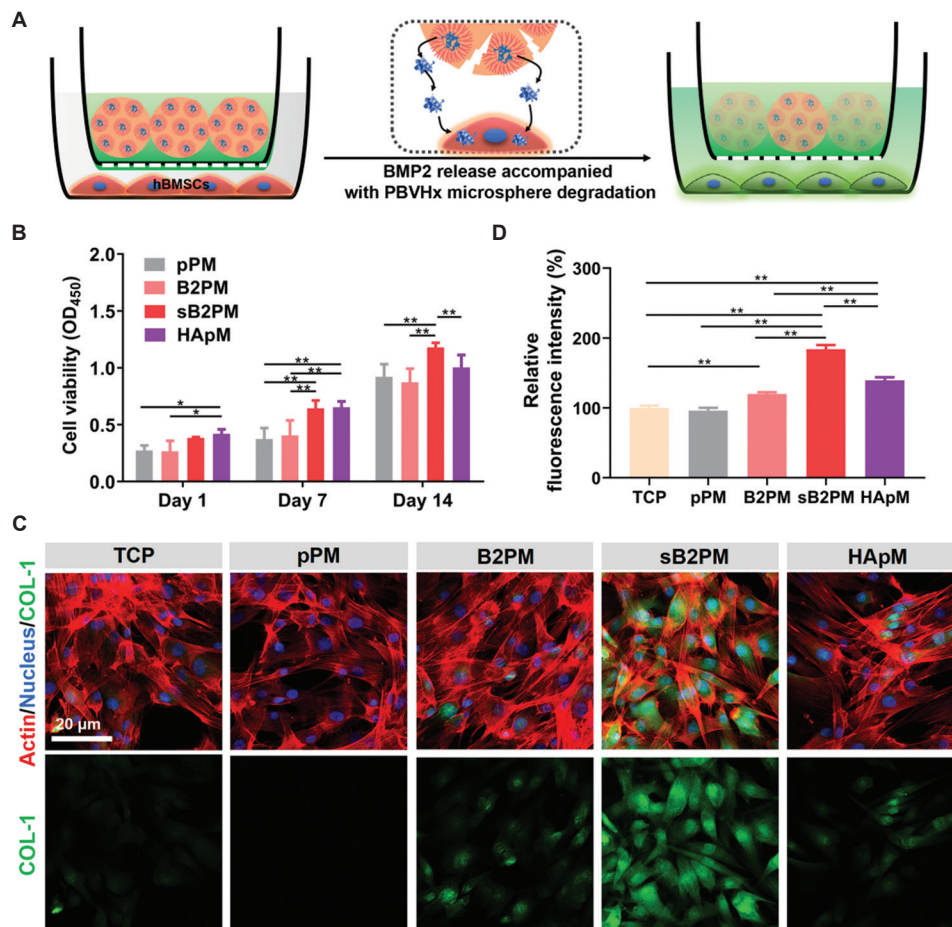
Figure 4. *In vitro* cytotoxicity and biocompatibility of sB2PM microspheres. (A) Schematic of *in vitro* co-culture system of pPM, B2PM, and sB2PM with primary hBMSCs. (B) Viability of primary hBMSCs co-cultured with pPM, B2PM, and sB2PM. (C) Confocal laser scanning microscopy images of primary hBMSCs co-cultured with pPM, B2PM, and sB2PM labeled with COL1A1 (green fluorescent), actin (red fluorescent), and DAPI (blue fluorescent). Scale bar = 20 μm. (D) Quantification of the mean intensity for green immunofluorescence staining. Data are presented as mean ± SD (n=3). *p<0.05, **p<0.01.

Abbreviations: BMP2: Bone morphogenetic protein-2; B2PM: PBVHx/BMP2 controlled-release microspheres; COL-1: Collagen type I; HApM: Commercial hydroxyapatite microspheres; hBMSCs: Human bone marrow-derived mesenchymal stem cells; OD: Optical density; PBVHx: Poly(3-hydroxybutyrate-co-3-hydroxyvalerate-co-3-hydroxyhexanoate); pPM: Pure PBVHx-based microspheres; sB2PM: PBVHx/soy lecithin (SL)/BMP2 controlled-release microspheres; TCP: Tissue culture plate.

was reduced in HLU mice, was also significantly restored by sB2PM treatment, outperforming HApM (**Figure 6J** and **K**).

Histopathological features of the femur were further examined using H&E and MT staining. H&E staining showed that cancellous bone structure remained intact in control mice but was significantly compromised in HLU mice. Treatment with sB2PM significantly improved cancellous bone mass (**Figure 7A** and **C**). MT staining revealed that collagen fiber deposition by mature osteoblasts was reduced in the HLU group but significantly increased following sB2PM treatment (**Figure 7A** and **D**). To further elucidate the mechanism underlying the bone-regenerative effects of sB2PM, immunohistochemical staining for osteogenic markers ALP and RUNX2 was performed. Compared to the PBS group, pPM and HApM slightly increased ALP and RUNX2 expression. In contrast, the sB2PM group showed significantly higher expression of both proteins, indicating that BMP2-coated sB2PM possesses strong bone-regenerative properties *in vivo* (**Figure 7B**, **E**, and **F**). Taken together, these

results suggest that sB2PM effectively reduces HLU-induced bone loss and promotes osteogenic differentiation and bone regeneration by upregulating osteoblast-related transcription factors, such as RUNX2 and ALP activity, thereby alleviating disuse osteoporosis *in vivo*.

4. Discussion

In this study, we captured BMP2 using SL and fabricated composite microspheres with the biodegradable material PBVHx to achieve efficient encapsulation and controlled biphasic release of BMP2. At the cellular level, it was confirmed that sB2PM exhibits good biocompatibility and can promote hBMSC proliferation and collagen secretion. In a mouse model of disuse osteoporosis, injectable sB2PM modulated collagen secretion, as well as ALP and RUNX2 expression, thereby alleviating osteoporotic bone defects. This study provides a new strategy for bone regeneration therapy in osteoporosis.

In bone tissue engineering, 3HB, P(3HB-co-4HB), and PHBHHx have been used for osteogenic differentiation and
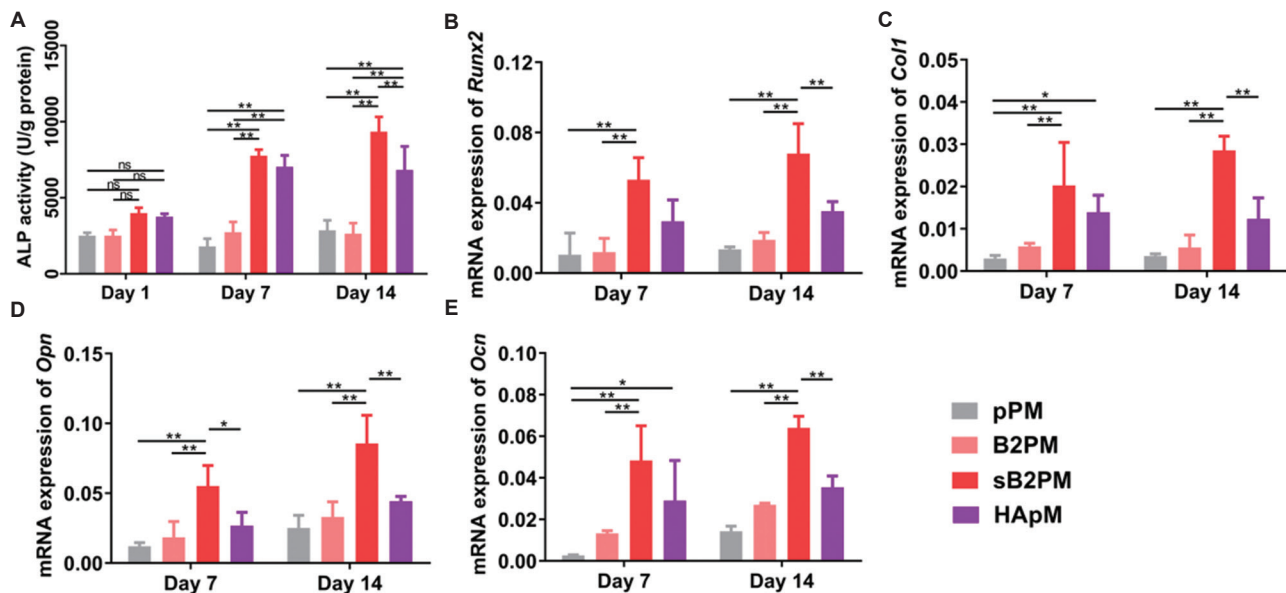
Figure 5. Effect of sB2PM on the osteogenic differentiation of hBMSCs *in vitro*. (A) ALP activity assay of hBMSCs co-cultured with pPM, B2PM, and sB2PM on days 1, 7, and 14. (B–E) Real-time polymerase chain reaction analysis of *Runx2*, *Col1*, *Opn*, and *Ocn* expression in hBMSCs co-cultured with pPM, B2PM, and sB2PM on days 7 and 14. Data are presented as mean ± SD (n=3). *p<0.05, **p<0.01.
Abbreviations: ALP: Alkaline phosphatase; B2PM: PBVHx/BMP2 controlled-release microspheres; *Col1*: Collagen type I; HApM: Commercial hydroxyapatite microspheres; hBMSCs: Human bone marrow-derived mesenchymal stem cells; *Ocn*: Osteocalcin; *Opn*: Osteopontin; pPM: Pure PBVHx-based microspheres; *Runx2*: Runt-related transcription factor 2; sB2PM: PBVHx/soy lecithin (SL)/BMP2 controlled-release microspheres.

osteoporosis treatment.[24] However, the biological effects of PBVHx and its composites in bone defect repair have not been well elucidated. In this work, we combined PBVHx and BMP2 to form composite microspheres using SL, addressing the challenge of capturing and retaining the bioactivity of growth factors, such as BMP2. This approach is consistent with previous reports on the use of SL in stabilizing high drug loading.[44] Due to its high stability and availability, SL can protect BMPs from organic solvent-induced denaturation, thereby enabling the development of a sustained-release delivery system for cell growth factors.[45,46] In our research, the BMP2 encapsulation efficiency of sB2PM containing SL reached 80.29%, while B2PM without SL achieved only 16.08% (**Figure 2E**). The size and distribution of sB2PM were comparable to those of the pPM and B2PM groups; however, sB2PM exhibited a significantly granular surface morphology, likely due to the high SL and BMP2 loading. The hydrophilicity of the microspheres was evaluated via water absorption rate. A higher water uptake rate indicates greater hydrophilicity.[47] The results showed that sB2PM had the highest water uptake rate, indicating the strongest hydrophilicity, while pPM had the lowest (**Figure 2F**). However, the porosities among the three types of microspheres were similar (**Figure 2G**). These differences in hydrophilicity are likely due to SL or sB2 incorporation into the nanopores of the microspheres, altering their surface properties. Controlled release of BMP2 is the key to bone regeneration drug delivery systems.[48] sB2PM released BMP2 into the environment in two stages: An initial burst of BMP2 from the microsphere surface, followed by a sustained release through PBVHx degradation (**Figure 3E**). BMP2 localization in sB2PM was visualized by immunofluorescence

using a BMP2 antibody (**Figure 3A**). The fluorescence intensity on the surface of BMP2 was significantly higher than that of B2PM, confirming BMP2 loading (**Figure 3B**). In addition, sB2PM sustained BMP2 release for over 30 days, while B2PM released only a small amount within the first 12 h (**Figure 3D**). Notably, both microsphere types exhibited similar degradation behavior (**Figure 3C**).

In addition to excellent BMP2 loading and release capabilities, sB2PM also demonstrated good biocompatibility and osteoinductive properties. Results from cell proliferation experiments showed that sB2PM significantly promoted the proliferation of co-cultured hBMSCs cells at days 7 and 14 compared with pPM and B2PM, indicating the effectiveness of sB2PM in enabling the long-term, sustained release of BMP2. To evaluate the *in vitro* biological effects of BMP2 released from the microsphere system, the cytotoxicity of microspheres toward hBMSCs was assessed. Typically, microspheres and cells are separated using a Transwell system, with hBMSCs cultured in the lower chamber. The effects of the microspheres on hBMSC activity were evaluated using the CCK-8 assay after culturing in different microsphere-conditioned medium for 1, 7, and 14 days. During the experiment, the culture medium was changed daily. The cell viability in the sB2PM group was significantly higher than in the pPM and B2PM groups and also higher than that in the group treated with commercial HApM, indicating that the released BMP2 retained good biological activity and contributed to enhanced cell proliferation (**Figure 4B**). PHA materials are known to exhibit good biocompatibility with mesenchymal stem cells,[36,49] a finding that was also confirmed in our study. The ECM is involved in modulating cell responses to growth factors, including the
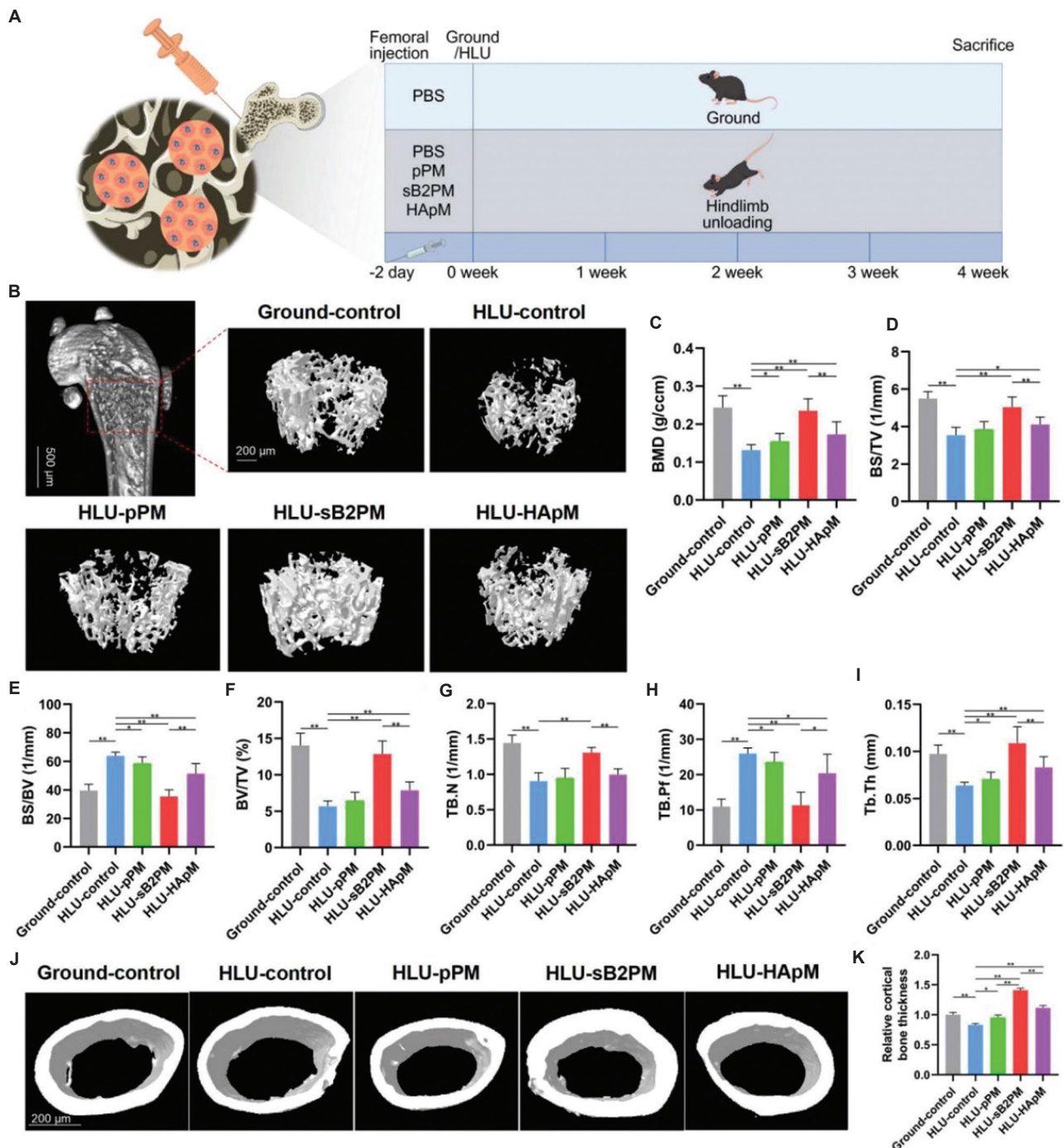
Figure 6. Protective effects of sB2PM on bone loss in disuse osteoporosis mice *in vivo*. (A) Experimental schedule for the construction of HLU-induced osteoporosis mouse model and the administration of pPM, B2PM, sB2PM, and HApM. (B) Representative 3D micro-CT reconstructions of femoral cancellous bone in HLU-induced osteoporotic mice, four weeks after treatment. Scale bar = 200 μm. (C–I) Quantitative analyses of BMD, BS/TV, BS/BV, BV/TV, TB.N, TB.Pf, and Tb.Th. (J) Representative 3D micro-CT reconstructions of femoral cortical bone in HLU mice. Scale bar = 200 μm. (K) Quantitative analysis of cortical bone thickness. Data are presented as mean ± SD (*n*=4). *$p < 0.05$, **$p < 0.01$.
Abbreviations: BMD: Bone mineral density; B2PM: PBVHx/BMP2 controlled-release microspheres; BS: Bone surface; BV: Bone volume; HApM: Commercial hydroxyapatite microspheres; hBMSCs: Human bone marrow-derived mesenchymal stem cells; HLU: Hindlimb unloading; micro-CT: Micro-computed tomography; PBS: Phosphate-buffered saline; pPM: Pure PBVHx-based microspheres; sB2PM: PBVHx/soy lecithin (SL)/BMP2 controlled-release microspheres; TB.N: Trabecular number; TB.Pf: Trabecular pattern factor; Tb.Th: Trabecular thickness; TV: Tissue volume.

regulation of adhesion, proliferation, differentiation, and the eventual formation of mature bone tissue.[50] Actin staining and COL1A1 immunofluorescence staining revealed that hBMSCs treated with sB2PM microspheres displayed an

elongated spindle-shaped morphology and good adhesion properties (**Figure 4C**). Moreover, the expression levels of COL1A1 followed the trend: sB2PM > B2PM ≈ HApM > pPM ≈ TCP (**Figure 4D**). Notably, sB2PM promoted greater
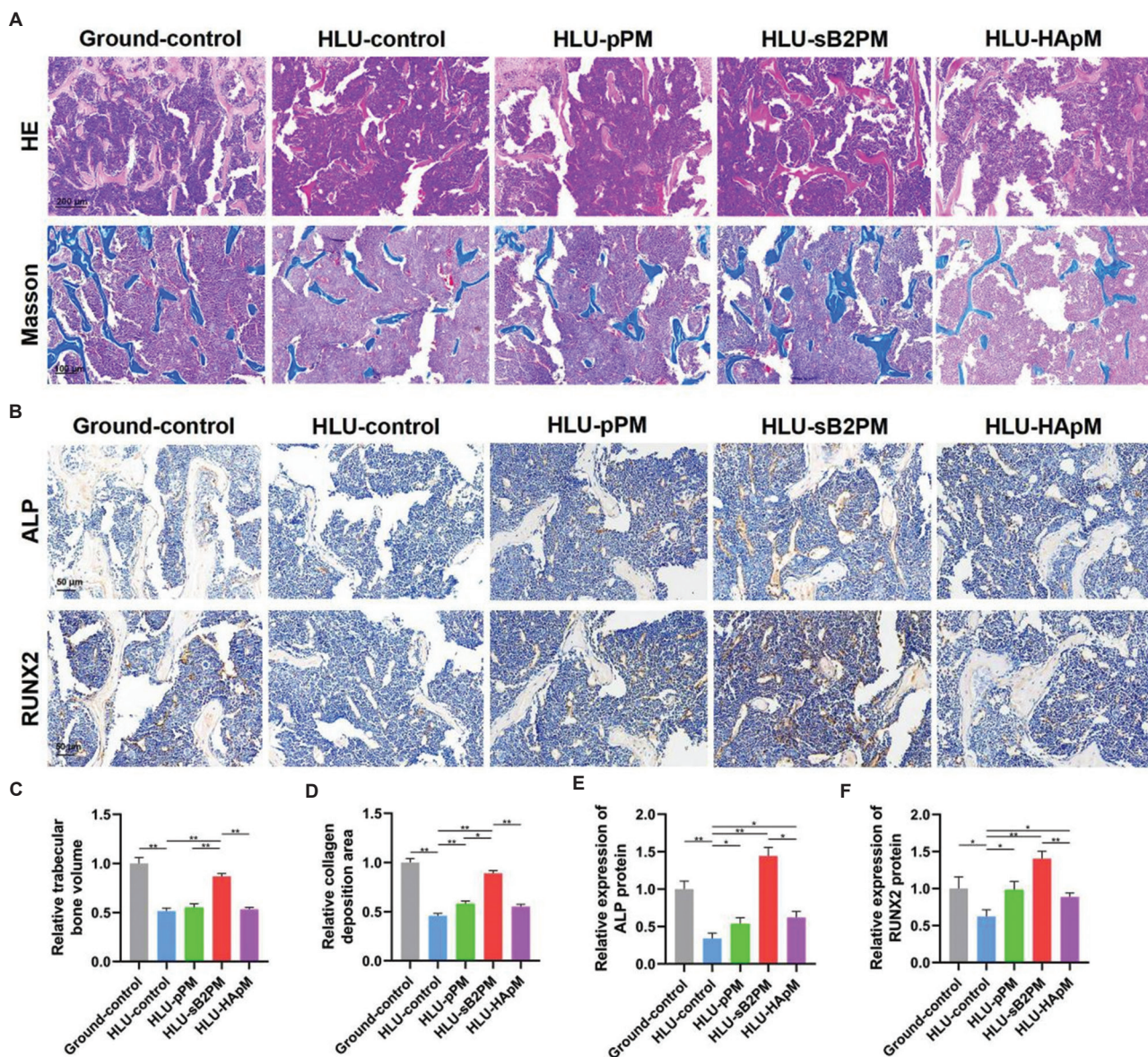
Figure 7. Mechanism of sB2PM in promoting bone regeneration in disuse osteoporosis mice *in vivo*. (A) Representative HE and Masson's trichrome staining images of femoral sections from HLU-induced osteoporotic mice treated with pPM, B2PM, sB2PM, and HApM. Scale bars = 200 μm (upper) and 100 μm (lower). (B) Representative immunohistochemical staining images of ALP and RUNX2 in femoral sections of HLU-induced osteoporotic mice administrated with various formulations. Scale bar = 50 μm. (C) Quantitative analysis of trabecular bone volume. (D) Quantitative analysis of collagen deposition area. (E) Quantification of immunohistochemical staining intensity for ALP and RUNX2. Data are presented as mean ± SD (*n*=4). *$p < 0.05$, **$p < 0.01$.

Abbreviations: ALP: Alkaline phosphatase; B2PM: PBVHx/BMP2 controlled-release microspheres; HApM: Commercial hydroxyapatite microspheres; HE: Hematoxylin and eosin; HLU: Hindlimb unloading; pPM: Pure PBVHx-based microspheres; RUNX2: Runt-related transcription factor 2; sB2PM: PBVHx/soy lecithin (SL)/BMP2 controlled-release microspheres.

cell proliferation than HApM after 14 days of co-culture, and also induced higher COL1A1 secretion. Previous studies have shown that hydroxyapatite is an important osteoinductive component.[51-53] These results indicate that sB2PM exhibits superior cell growth support and ECM secretion capacity compared to HApM.

To verify the activity of sB2PM in promoting osteogenic differentiation of hBMSCs, we further evaluated ALP activity and expression of osteogenic differentiation genes in hBMSCs co-cultured with various microspheres at different time points (**Figure 5**). ALP activity is an important indicator for assessing

the osteogenic differentiation of mesenchymal stem cells.[54,55] The current findings showed that on day 1, ALP activity across all five groups was similar. By day 7, ALP activity in the sB2PM and HApM groups was comparable but higher than that in the other groups. At day 14, the ALP activity in the sB2PM group exceeded that in all other groups (**Figure 5A**). In addition, *Runx2*, a key transcription factor and an important marker of osteogenic differentiation, promotes the expression of COL-1 and OCN in the early stages of differentiation.[56,57] COL-1 and OPN are metaphase marker genes, where COL-1 expression increases when osteoblasts begin synthesizing and secreting

ECM, while OPN is involved in bone matrix mineralization. OCN is a late-stage marker gene expressed when osteoblasts reach maturity.[58,59] Consistent with the ALP activity results, by day 14, the expression levels of osteogenic genes (*Runx2*, *Col1*, *Opn*, and *Ocn*) were all significantly upregulated in the sB2PM group compared to the other groups. This indicates that sB2PM microspheres have strong osteoinductive potential. Moreover, the osteogenic effect of s2BPM was significantly greater than that of HApM, which aligns with the results observed for cell proliferation and ECM secretion.

To confirm the therapeutic effect of sB2PM on osteoporotic bone defects *in vivo*, we established a mouse disuse osteoporosis model by tail suspension (HLU) and assessed the alleviating effect of sB2PM on osteoporosis four weeks post-modeling (**Figure 6A**). Micro-CT analysis revealed that sB2PM significantly increased bone mass in HLU mice compared with PBS, pPM, and HApM groups, with recovery levels comparable to those of the ground control group. These results indicate that sB2PM exhibits strong osteoinductive properties (**Figure 6B-K**). Furthermore, H&E and MT staining confirmed the excellent performance of sB2PM in promoting bone regeneration and collagen deposition. Immunohistochemical analysis also showed a significant increase in the expression of ALP and RUNX2 in bone tissues (**Figure** 7). These findings are consistent with the *in vitro* results for cell proliferation and osteogenic differentiation. To our knowledge, this study is the first to employ PBVHx as a controlled-release carrier for BMP2 in the treatment of osteoporotic bone defects, highlighting its innovative potential. *In vitro* results confirmed the robust osteoinductive activity of sB2PM. Furthermore, *in vivo* findings demonstrated that sB2PM significantly attenuated HLU-induced bone loss by upregulating key osteogenic markers (ALP and RUNX2), outperforming commercial HApM. Collectively, these results provide compelling evidence that the BMP2-sustained release system based on PBVHx-based microspheres represents a promising osteoinductive platform for future bone regeneration applications.

5. Conclusion

In the present study, we developed a novel biodegradable PBVHx composite microsphere (sB2PM) capable of promoting the osteogenic differentiation of mesenchymal stem cells and enhancing bone regeneration. The composite incorporates SL-linked BMP2, which provides a high BMP2 loading capacity and sustained, controlled-release ability. This design reduces the frequency of administration *in vivo* while maintaining the biological activity of BMP2 and improving its bone regenerative effects. *In vitro* experiments showed that sB2PM effectively promotes the proliferation and osteogenic differentiation of hBMSCs and regulates the expression of both early and late-stage osteogenic markers, such as *Runx2*, *Col1*, *Opn*, and *Ocn*. *In vivo* studies further confirmed that sB2PM significantly enhances the regeneration of both cancellous and cortical bone in HLU mice and modulates collagen secretion as well as the expression of ALP and RUNX2 proteins. These findings highlight the potential of BMP2 delivery systems based on biodegradable PBVHx microspheres for bone regeneration,

providing promising strategies for applications in bone tissue engineering, aerospace medical engineering, drug delivery, and beyond.

Conflicts of interest statement
The authors declare no potential conflicts of interest with respect to the research, authorship, and/or publication of this work.

Author contributions
Conceptualization: DW and XL; *Data curation*: KZ and YZ; *Investigation*: KZ, YZ, DW, and XL; *Methodology*: KZ and YZ; *Project administration*: DW and XL; *Resource*s: DW and XL; *Supervision*: DW and XL; *Writing – original draft*: KZ, YZ, DW, and XL; *Writing – review & editing*: AQ, DW, and XL. All authors reviewed and approved the final version of the manuscript.

Ethics approval and consent to participate
All animal experimental protocols were approved by the Medical and Laboratory Animal Ethics Committee of Northwestern Polytechnical University (China).

Consent for publication
Not applicable.

Availability of data
Data from this study are available from the corresponding author upon reasonable request.

References

1. Song S, Guo Y, Yang Y, Fu D. Advances in pathogenesis and therapeutic strategies for osteoporosis. *Pharmacol Ther*. 2022;237:108168. doi: 10.1016/j.pharmthera.2022.108168

2. Lin X, Zhang K, Li Y, *et al*. High resolution osteoclast-targeted imaging-guided osteoporosis alleviation via persistent luminescence nanocomposite. *Chem Eng J*. 2024;484:149468. doi: 10.1016/j.cej.2024.149468

3. Bian Y, Hu T, Lv Z, *et al*. Bone tissue engineering for treating osteonecrosis of the femoral head. *Exploration (Beijing)*. 2023;3(2):20210105. doi: 10.1002/exp.20210105

4. Liu H, Su J. Organoid and organoid extracellular vesicles for osteoporotic fractures therapy: Current status and future perspectives. *Interdiscipl Med*. 2023;1(3):e20230011. doi: 10.1002/INMD.20230011

5. Xue C, Chen L, Wang N, *et al*. Stimuli-responsive hydrogels for bone tissue engineering. *Biomater Transl*. 2024;5(3):257-273. doi: 10.12336/biomatertransl.2024.03.004

6. Hayashi K, Zhang C, Taleb Alashkar AN, Ishikawa K. Carbonate apatite honeycomb scaffold-based drug delivery system for repairing osteoporotic bone defects. *ACS Appl Mater Interfaces*. 2024;16(35):45956-45968. doi: 10.1021/acsami.4c08047

7. Zhou J, Zhang Z, Joseph J, *et al*. Biomaterials and nanomedicine for bone regeneration: Progress and future prospects. *Exploration (Beijing)*. 2021;1(2):20210011.

doi: 10.1002/exp.20210011

8. Liu A, Yang G, Zhao Y, *et al.* Bone-targeted hybrid extracellular vesicles for alveolar bone regeneration. *Interdiscip Med.* 2025:e20240126.
    doi: 10.1002/INMD.20240126

9. Li Y, Zhang H, Jiang Y, Yang J, Cai D, Bai X. The application of extracellular vesicles in orthopedic diseases. *Interdiscip Med.* 2024;2(3):e20230055.
    doi: 10.1002/INMD.20230055

10. Zhang Y, Li D, Liu Y, *et al.* 3D-bioprinted anisotropic bicellular living hydrogels boost osteochondral regeneration via reconstruction of cartilage-bone interface. *Innovation (Camb).* 2024;5(1):100542.
    doi: 10.1016/j.xinn.2023.100542

11. Hu Q, Pan X, Liang Y, *et al.* Comparative efficacy and safety of bisphosphonate therapy for bone loss in individuals after middle age: A systematic review and network meta-analysis. *Nano TransMed.* 2022;1(1):e9130003.
    doi: 10.26599/NTM.2022.9130003

12. Rossini M, Bianchi G, Di Munno O, *et al.* Determinants of adherence to osteoporosis treatment in clinical practice. *Osteoporos Int.* 2006;17(6):914-921.
    doi: 10.1007/s00198-006-0073-6

13. Wang Y, Sun L, Kan T, *et al.* Hypermethylation of Bmp2 and Fgfr2 promoter regions in bone marrow mesenchymal stem cells leads to bone loss in prematurely aged mice. *Aging Dis.* 2024;16(2):1149-1168.
    doi: 10.14336/AD.2024.0324

14. Yu YL, Martens DS, An DW, *et al.* Osteoporosis in relation to a bone-related aging biomarker derived from the urinary proteomic profile: A population study. *Aging Dis.* 2024;16(1):633.
    doi: 10.14336/AD.2024.0303

15. Bai L, Song P, Su J. Bioactive elements manipulate bone regeneration. *Biomater Transl.* 2023;4(4):248.
    doi: 10.12336/biomatertransl.2023.04.005

16. Zhang P, Qin Q, Cao X, *et al.* Hydrogel microspheres for bone regeneration through regulation of the regenerative microenvironment. *Biomater Transl.* 2024;5(3):205-235.
    doi: 10.12336/biomatertransl.2024.03.002

17. Salazar VS, Gamer LW, Rosen V. BMP signalling in skeletal development, disease and repair. *Nat Rev Endocrinol.* 2016;12(4):203-221.
    doi: 10.1038/nrendo.2016.12

18. Zhou N, Li Q, Lin X, *et al.* BMP2 induces chondrogenic differentiation, osteogenic differentiation and endochondral ossification in stem cells. *Cell Tissue Res.* 2016;366(1):101-111.
    doi: 10.1007/s00441-016-2403-0

19. Rahman M, Peng XL, Zhao XH, *et al.* 3D bioactive cell-free-scaffolds for *in-vitro/in-vivo* capture and directed osteoinduction of stem cells for bone tissue regeneration. *Bioact Mater.* 2021;6(11):4083-4095.
    doi: 10.1016/j.bioactmat.2021.01.013

20. Rosen V. BMP2 signaling in bone development and repair. *Cytokine Growth Factor Rev.* 2009;20(5-6):475-480.
    doi: 10.1016/j.cytogfr.2009.10.018

21. Rodda SJ, McMahon AP. Distinct roles for Hedgehog and canonical Wnt signaling in specification, differentiation and maintenance of osteoblast progenitors. *Development.* 2006;133(16):3231-3244.
    doi: 10.1242/dev.02480

22. Albert SG, Reddy S. Clinical evaluation of cost efficacy of drugs for treatment of osteoporosis: A meta-analysis. *Endocr Pract.* 2017;23(7):841-856.
    doi: 10.4158/EP161678.RA

23. Liang W, Zhou C, Liu X, *et al.* Current status of nano-embedded growth factors and stem cells delivery to bone for targeted repair and regeneration. *J Orthop Translat.* 2025;50:257-273.
    doi: 10.1016/j.jot.2024.12.006

24. Fu Z, Qiu H, Xu Y, Tan C, Wang H. Biological effects, properties and tissue engineering applications of polyhydroxyalkanoates: A review. *Int J Biol Macromol.* 2025;293:139281.
    doi: 10.1016/j.ijbiomac.2024.139281

25. Ding YW, Li Y, Zhang ZW, Dao JW, Wei DX. Hydrogel forming microneedles loaded with VEGF and Ritlecitinib/polyhydroxyalkanoates nanoparticles for mini-invasive androgenetic alopecia treatment. *Bioactive Mater.* 2024;38:95-108.

26. Ren ZW, Wang ZY, Ding YW, *et al.* Polyhydroxyalkanoates: The natural biopolyester for future medical innovations. *Biomater Sci.* 2023;11(18):6013-6034.
    doi: 10.1039/d3bm01043k

27. Xu T, Huang XY, Dao JW, Xiao D, Wei DX. Synthetic biology for medical biomaterials. *Interdiscip Med.* 2025;3:e20240087.
    doi: 10.1002/INMD.20240087

28. Luo Q, Zou F, Yang D, *et al.* The production and characterization of an aminolyzed polyhydroxyalkanoate membrane and its cytocompatibility with osteoblasts. *Molecules.* 2025;30(4):950.
    doi: 10.3390/molecules30040950

29. Zhao Y, Zou B, Shi Z, Wu Q, Chen GQ. The effect of 3-hydroxybutyrate on the *in vitro* differentiation of murine osteoblast MC3T3-E1 and *in vivo* bone formation in ovariectomized rats. *Biomaterials.* 2007;28(20):3063-3073.
    doi: 10.1016/j.biomaterials.2007.03.003

30. Cao Q, Zhang J, Liu H, Wu Q, Chen J, Chen GQ. The mechanism of anti-osteoporosis effects of 3-hydroxybutyrate and derivatives under simulated microgravity. *Biomaterials.* 2014;35(28):8273-8283.
    doi: 10.1016/j.biomaterials.2014.06.020

31. Wei DX, Chen Z. Current situation and challenge of exogenous 3-hydroxybutyrate derived from polyhydroxyalkanoates for elderly health: A review. *Int J Biol Macromol.* 2025;285:138328.
    doi: 10.1016/j.ijbiomac.2024.138328

32. Esmaeili M, Ghasemi S, Shariati L, Karbasi S. Evaluating the osteogenic properties of polyhydroxybutyrate-zein/multiwalled carbon nanotubes (MWCNTs) electrospun composite scaffold for bone tissue engineering applications. *Int J Biol Macromol.* 2024;276(Pt 2):133829.
    doi: 10.1016/j.ijbiomac.2024.133829

33. Wei DX, Dao JW, Chen GQ. A Micro-Ark for cells: Highly open porous polyhydroxyalkanoate microspheres as injectable scaffolds for tissue regeneration. *Adv Mater.* 2018;30(31):e1802273.
    doi: 10.1002/adma.201802273

34. Li J, Zhang X, Peng ZX, *et al.* Metabolically activated energetic materials mediate cellular anabolism for bone regeneration. *Trends Biotechnol.* 2024;42(12):1745-1776.
    doi: 10.1016/j.tibtech.2024.08.002

35. Hu YJ, Wei X, Zhao W, Liu YS, Chen GQ. Biocompatibility of poly(3-hydroxybutyrate-co-3-hydroxyvalerate-co-3-hydroxyhexanoate) with bone marrow mesenchymal stem cells. *Acta Biomater.* 2009;5(4):1115-1125.
    doi: 10.1016/j.actbio.2008.09.021

36. Su Z, Li P, Wu B, *et al.* PHBVHHx scaffolds loaded with umbilical cord-derived mesenchymal stem cells or hepatocyte-like cells differentiated from these cells for liver tissue engineering. *Mater Sci Eng C Mater Biol Appl.* 2014;45:374-382.
    doi: 10.1016/j.msec.2014.09.022

37. Hu J, Wang M, Xiao X, *et al.* A novel long-acting azathioprine polyhydroxyalkanoate nanoparticle enhances treatment efficacy for systemic lupus erythematosus with reduced side effects. *Nanoscale.* 2020;12(19):10799-10808.
    doi: 10.1039/d0nr01308k

38. Wei DX, Cai D, Tan Y, *et al.* Poly (3-hydroxybutyrate-co-3-hydroxyvalerate-co-3-hydroxyhexanoate)-based microspheres as a sustained platform for Huperzine A delivery for Alzheimer's disease therapy. *Int J Biol Macromol.* 2024;282:136582.
    doi: 10.1016/j.ijbiomac.2024.136582

39. Huang XY, Zhou XX, Yang H, *et al.* Directed osteogenic differentiation of human bone marrow mesenchymal stem cells via sustained release of BMP4 from PBVHx-based nanoparticles. *Int J Biol Macromol.* 2024;265:130649.
    doi: 10.1016/j.ijbiomac.2024.130649

40. Zhou XX, Huang XY, Zhang M, *et al.* A BMP6 supply system based on PBVHx nanoparticles promotes the osteogenic differentiation of human stem cells in simulated microgravity. *Int J Biol Macromol.* 2025;319:145444.
    doi: 10.1016/j.ijbiomac.2025.145444

41. Mi CH, Qi XY, Ding YW, Zhou J, Dao JW, Wei DX. Recent advances of medical polyhydroxyalkanoates in musculoskeletal system. *Biomater Transl.* 2023;4(4):234-247.

doi: 10.12336/biomatertransl.2023.04.004

42. Zhao XH, Peng XL, Gong HL, Wei DX. Osteogenic differentiation system based on biopolymer nanoparticles for stem cells in simulated microgravity. *Biomed Mater.* 2021;16(4):044102.
doi: 10.1088/1748-605X/abe9d1

43. Cai H, Han XJ, Luo ZR, *et al.* Pretreatment with Notoginsenoside R1 enhances the efficacy of neonatal rat mesenchymal stem cell transplantation in model of myocardial infarction through regulating PI3K/Akt/FoxO1 signaling pathways. *Stem Cell Res Ther.* 2024;15(1):419.
doi: 10.1186/s13287-024-04039-x

44. Li H, Liu B, Ao H, *et al.* Soybean lecithin stabilizes disulfiram nanosuspensions with a high drug-loading content: remarkably improved antitumor efficacy. *J Nanobiotechnology.* 2020;18(1):4.
doi: 10.1186/s12951-019-0565-0

45. Xue Y, Li Y, Zhang D, Xu W, Ning C, Han D. Calcium phosphate silicate microspheres with soybean lecithin as a sustained-release bone morphogenetic protein-delivery system for bone tissue regeneration. *ACS Biomater Sci Eng.* 2023;9(5):2596-2607.
doi: 10.1021/acsbiomaterials.2c01065

46. Chen R, Yu J, Gong HL, *et al.* An easy long-acting BMP7 release system based on biopolymer nanoparticles for inducing osteogenic differentiation of adipose mesenchymal stem cells. *J Tissue Eng Regen Med.* 2020;14(7):964-972.
doi: 10.1002/term.3070

47. Wei D, Qiao R, Dao J, *et al.* Soybean lecithin-mediated nanoporous PLGA microspheres with highly entrapped and controlled released BMP-2 as a stem cell platform. *Small.* 2018;14(22):e1800063.
doi: 10.1002/smll.201800063

48. Yang Z, Li X, Gan X, *et al.* Hydrogel armed with Bmp2 mRNA-enriched exosomes enhances bone regeneration. *J Nanobiotechnol.* 2023;21(1):119.
doi: 10.1186/s12951-023-01871-w

49. Sriram M, Priya S, Katti DS. Polyhydroxybutyrate-based osteoinductive mineralized electrospun structures that mimic components and tissue interfaces of the osteon for bone tissue engineering. *Biofabrication.* 2024;16(2):025036.
doi: 10.1088/1758-5090/ad331a

50. Lin X, Patil S, Gao YG, Qian A. The bone extracellular matrix in bone formation and regeneration. *Front Pharmacol.* 2020;11:757.
doi: 10.3389/fphar.2020.00757

51. Fendi F, Abdullah B, Suryani S, Usman AN, Tahir D. Development and application of hydroxyapatite-based scaffolds for bone tissue regeneration: A systematic literature review. *Bone.* 2024;183:117075.
doi: 10.1016/j.bone.2024.117075

52. Bystrov V, Bystrova A, Dekhtyar Y. HAP nanoparticle and substrate surface electrical potential towards bone cells adhesion: Recent results review. *Adv Colloid Interface Sci.* 2017;249:213-219.
doi: 10.1016/j.cis.2017.05.002

53. Wan B, Ruan Y, Shen C, *et al.* Biomimetically precipitated nanocrystalline hydroxyapatite. *Nano TransMed.* 2022;1(2-4):e9130008.
doi: 10.26599/NTM.2022.9130008

54. Makris K, Mousa C, Cavalier E. Alkaline phosphatases: Biochemistry, functions, and measurement. *Calcif Tissue Int.* 2023;112(2):233-242.
doi: 10.1007/s00223-022-01048-x

55. Lin Z, Chen Z, Chen Y, *et al.* Hydrogenated silicene nanosheet functionalized scaffold enables immuno-bone remodeling. *Exploration (Beijing).* 2023;3(4):20220149.
doi: 10.1002/exp.20220149

56. Li H, Fan J, Fan L, *et al.* MiRNA-10b reciprocally stimulates osteogenesis and inhibits adipogenesis partly through the TGF-β/SMAD2 signaling pathway. *Aging Dis.* 2018;9(6):1058.
doi: 10.14336/AD.2018.0214

57. Sharma G, Lee YH, Kim JC, Sharma AR, Lee SS. Bone regeneration enhanced by quercetin-capped selenium nanoparticles via miR206/Connexin43, WNT, and BMP signaling pathways. *Aging Dis.* 2026;17(1):2.

58. Zhu S, Chen W, Masson A, Li YP. Cell signaling and transcriptional regulation of osteoblast lineage commitment, differentiation, bone formation, and homeostasis. *Cell Discov.* 2024;10(1):71.
doi: 10.1038/s41421-024-00689-6

59. Jin F, Liu M, Zhang D, Wang X. Translational perspective on bone-derived cytokines in inter-organ communications. *Innovation (Camb).* 2023;4(1):100365.
doi: 10.1016/j.xinn.2022.100365